









## Article

# Temporal Vine Water Status Modeling Through Machine Learning Ensemble Technique and Sentinel-2 Multispectral Images Under Semi-Arid Conditions

Vincenzo Giannico <sup>1,†</sup> , Simone Pietro Garofalo <sup>2,\*,†</sup> , Luca Brillante <sup>3</sup>, Pietro Sciusco <sup>4</sup>, Mario Elia <sup>1</sup> , Giuseppe Lopriore <sup>1</sup> , Salvatore Camposeo <sup>1</sup> , Raffaele Laforteza <sup>1</sup> , Giovanni Sanesi <sup>1</sup>  and Gaetano Alessandro Vivaldi <sup>1</sup> 

<sup>1</sup> Department of Soil, Plant and Food Sciences, University of Bari A. Moro, Via Amendola 165/A, 70126 Bari, Italy; vincenzo.giannico@uniba.it (V.G.); giuseppe.lopriore@uniba.it (G.L.); salvatore.camposeo@uniba.it (S.C.); gaetano.vivaldi@uniba.it (G.A.V.)

<sup>2</sup> Council for Agricultural Research and Economics, Research Centre for Agriculture and Environment, Via Celso Ulpiani 5, 70125 Bari, Italy

<sup>3</sup> Department of Viticulture & Enology, California State University Fresno, Fresno, CA 93740, USA

<sup>4</sup> Planetek Italia, Via Massaua 12, 70132 Bari, Italy

\* Correspondence: simone.garofalo@crea.gov.it

† These authors contributed equally to this work.

**Abstract:** New challenges will be experienced by the agriculture sector in the near future, especially due to the effects of climate change. For example, rising temperatures could result in increased evapotranspiration demand, causing difficulties in the management of irrigation practices. Generally, an important predictor of plant water status to be taken into account for irrigation monitoring and management is the stem water potential. However, it requires a huge amount of time-consuming fieldwork, particularly when an adequate data amount is necessary to fully investigate the spatial and temporal variability of large areas under monitoring. In this study, the integration of machine learning and satellite remote sensing (Sentinel-2) was investigated to obtain a model able to predict the stem water potential in viticulture using multispectral imagery. Vine water status data were acquired within a Montepulciano vineyard in the south of Italy (Puglia region), under semi-arid conditions; data were acquired over two years during the irrigation seasons. Different machine learning algorithms (lasso, ridge, elastic net, and random forest) were compared using vegetation indices and spectral bands as predictors in two independent analyses. The results show that it is possible to remotely estimate vine water status with random forest from vegetation indices ( $R^2 = 0.72$ ). Integrating machine learning techniques and satellite remote sensing could help farmers and technicians manage and plan irrigation, avoiding or reducing fieldwork.

**Keywords:** water scarcity; predictive modeling; Mediterranean environment; machine learning; precision farming; remote sensing; vine



**Citation:** Giannico, V.; Garofalo, S.P.; Brillante, L.; Sciusco, P.; Elia, M.; Lopriore, G.; Camposeo, S.; Laforteza, R.; Sanesi, G.; Vivaldi, G.A. Temporal Vine Water Status Modeling Through Machine Learning Ensemble Technique and Sentinel-2 Multispectral Images Under Semi-Arid Conditions. *Remote Sens.* **2024**, *16*, 4784. <https://doi.org/10.3390/rs16244784>

Academic Editors: Jiehao Li, Jochem Verrelst, Xiwen Luo, Shan Zeng and Chenguang Yang

Received: 31 October 2024

Revised: 19 December 2024

Accepted: 20 December 2024

Published: 22 December 2024



**Copyright:** © 2024 by the authors. Licensee MDPI, Basel, Switzerland. This article is an open access article distributed under the terms and conditions of the Creative Commons Attribution (CC BY) license (<https://creativecommons.org/licenses/by/4.0/>).

## 1. Introduction

In the near future, one of the most significant challenges for sustainable agriculture will undoubtedly be climate change; according to the projections by IPCC [1], a global temperature increase of 1.5 °C is expected by 2040. In this scenario, agriculture and food production systems will be increasingly vulnerable, especially in the poor areas of the world [2]. Irrigation management will assume a determining and central role due to the expected increase in evapotranspiration demand and water scarcity, resulting from higher temperatures and more frequent dry periods [3,4]. In Europe, vineyard cultivations tend to be rainfed; however, the future trend will be to irrigate more often trying to reduce the effects of climate change [5]; in fact, generally, good productivity

can be achieved in circumstances where soil and climate conditions do not represent limiting factors to photosynthetic activity. For instance, adequate temperatures, and no water stress; furthermore, climate change could also expose vineyards to an increased drought stress risk, with impacts on berry size and bud fertility [6–8]. Over the past few years, significant progress has been made to develop efficient irrigation methods and deficit irrigation strategies, improving the quality of grape berries and the efficiency of water use in vineyards cultivated in semi-arid regions [9]; to date, irrigation management in viticulture is generally based on the determination of vine water status, for example, through the measurement of the stem water potential. However, the relative procedure requires the use of field instruments (i.e., pressure chamber), time-consuming fieldwork campaigns, the presence of technical personnel in the field, and several samples per area to have a robust spatial estimation of vineyard water status. Therefore, the possibility of basing irrigation management on non-destructive methods that can give information over a large area, such as remote sensing technologies, could implement irrigation management in viticulture, guaranteeing spatially and temporally efficient crop water demand assessments [10]. In addition, increasing the geographic information system (GIS), e.g., QGIS applications in agriculture, is helping to map the existing variability of several parameters at the field and regional level [11,12]. Advances in agricultural remote sensing offer the possibility of detecting and monitoring different crop parameters by assessing temporal and spatial variability [8,13]. Spectral images from different platforms, such as drones and airborne, have been largely used to estimate crop parameters; nonetheless, the use of satellite images offers other advantages, such as the opportunity to more easily monitor crops, perform time-series analyses and, in some cases, images are provided for free (e.g., Sentinel-2 and Landsat 8 imagery). In viticulture, the application of satellite imagery has been extensively studied for monitoring water status using various data sources. Specifically, Helman et al. [14] utilized high-resolution satellite imagery (e.g., Planet) to estimate stem water potential (STEM) in vineyards. Their approach employed vegetation indices as predictors in a multiple linear regression model, which achieved robust performance ( $R^2 = 0.84$ ). Similarly, high-resolution multispectral UAV imagery combined with weather data has been used to map leaf water potential in Californian vineyards. Tang et al. ([15]) demonstrated significant correlations with ground measurements, employing a random forest (RF) model that explained 77% of the variance in leaf water potential ( $\psi_{\text{leaf}}$ ). Recent studies have also explored lower-resolution satellite sensors for assessing vine water status. For instance, Laroche-Pinel et al. ([16]) analyzed vine water status through field measurements of stem water potential from the pea-size stage to ripening using Sentinel-2 imagery. They applied various machine learning models to predict stem water potential, achieving a moderate  $R^2$  of 0.40. Additionally, Sentinel-2 imagery has been used to predict irrigated zones in the work of Esther López-Pérez et al. ([17]) Their study incorporated topographic and multispectral data into a random forest model in Spain, yielding highly accurate predictions (precision = 91.8%) of irrigated areas.

The scope of this study was to improve the detection and monitoring of vine water status through machine learning techniques and satellite images from the EU Earth observation program *Copernicus*, particularly from the Sentinel-2 satellite. Providing farmers and technicians with tools able to monitor vineyard water status could help them to reduce time-consuming and difficult fieldwork, providing the possibility to map field variability, with even greater representativeness than the typical proximal methods adopted to assess spatial and temporal crop variability. In this work, different machine learning algorithms (including lasso, ridge, elastic net, and random forest) were evaluated to predict the stem water potential in a vineyard grown under semi-arid conditions in the South of Italy. This research diverges from prior studies by utilizing solely Sentinel-2 imagery to estimate vine water status, addressing the limitations associated with the cost and accessibility of high-resolution data from UAVs or commercial satellites [18]. While thermal imaging has been effective for estimating vine water status at various scales (e.g., Bellvert et al. [19]), it typically requires more complex and expensive data acquisition systems. The high temporal resolution of Sentinel-2 facilitates

consistent monitoring, which is crucial for effective irrigation management. Furthermore, the application of machine learning techniques in this study enhances the predictive capability, providing a robust framework for precision viticulture [20].

## 2. Material and Methods

### 2.1. Site and Vineyard Description, Soil, and Meteorological Data

Measurements were taken in 2019 and 2020 in a commercial vineyard (*Vitis vinifera* L., cv. Montepulciano, grafted on Paulsen 1103 rootstock), situated near Andria (Apulia, South of Italy) (Latitude: 41°14'11.05"N; Longitude: 16°11'33.01"E; 142 m a.s.l.) (Figure 1). The vines were planted at a spacing of 2.30 m × 1.0 m (4348 vines/ha) and trained to a vertical trellis system (North–South oriented). The site area where measurements were acquired was about 2.40 ha. The soil of the site was classified as Sandy Loam, based on USDA classification. The vineyard was irrigated and fertilized according to the regional guidelines for sustainable crop management. The amount of irrigation water applied was 2951 m<sup>3</sup>/ha in 2019 and 2972 m<sup>3</sup>/ha in 2020 (the irrigation season started in June and ended in October in both years). Regional guidelines prescribed fertilization with 50 kg of N/ha, 40 kg of P<sub>2</sub>O<sub>5</sub>/ha, and 80 kg of K<sub>2</sub>O/ha. The agronomic practices used were those typical of the area, including, cutting back the tips of overly vigorous shoots after flowering, shoot trimming after the phenological phase of fruit set, and defoliation in the later stage of the grape cycle to enhance air circulation. The climate is Mediterranean with hot and dry summers and mildly cold winters; the average annual temperature is 15.8 °C, and the annual precipitation is approximately 566 mm [21]. Meteorological data collected over the two years in the experimental site were acquired from the Apulia region monitoring network [22].

### 2.2. Plant Water Status Determination

In 2019 and 2020, plant water status was determined by measuring the stem water potential (ΨSTEM; MPa) using a pressure chamber (Plant Water Status Console 3000F01, SOILMOISTURE CORP. Santa Barbara, CA, USA). Before ΨSTEM measurement, leaves were placed in aluminum foil for 60 min [9]; in both years, ΨSTEM data were acquired at midday (11.00 to 13.00 h solar). The experimental design consists of six plots, and, for each plot, 7 individual measurements were averaged to produce a single stem water potential value. Additionally, the measurements were taken across the following phenological phases: pea size, the beginning of bunch closure, berries still hard and green, berries beginning to color and enlarge, veraison, ripening, and harvest. Figure 1 shows the plots where the vines were located and on which ΨSTEM values were acquired; plots had different sizes due to inhomogeneity within the field.

### 2.3. Sentinel-2 Image Processing

All Sentinel-2 images covering the study area were downloaded for the years 2019 and 2020. Sentinel-2 consists of a constellation of two polar-orbiting satellites (Sentinel-2 A and B), in the same sun-synchronous orbit with overpass time at 10:30 a.m. local time, that carry a multispectral instrument (MSI) with 12 multispectral bands. Although Sentinel-2 is offered at multiple spatial resolutions of 10, 20, and 60 m, here, we used a spatial resolution of 20 m. Sentinel-2 images were downloaded as Level-2A, which provides atmospherically corrected Surface Reflectance (SR). Where Level-2A was not available, we downloaded Level-1C (i.e., top-of-atmosphere; TOA) images that were then atmospherically corrected to obtain SR by using the default settings of the Sen2Cor (v. 2.5.5) algorithm. We considered the spectral bands in the blue ("B02"), green ("B03"), red ("B04"), red-edge ("B05", "B06", and "B07"), near-infrared ("B8A"), and short-wave infrared ("B11" and "B12"). Only the images without clouds in the perimeter of the study area based on the cloud/snow detection algorithm developed by the European Space Agency [23] were selected for the study (27 images). In addition to the spectral bands, we also calculated 27 vegetation indices (VIs). The calculated VIs are reported in Table 1. Both VIs and biophysical parameters were

calculated using the Sentinel Application Platform (SNAP), a free tool provided by the ESA and developed for Earth observation, processing, and analysis of the Sentinel-2 images [24].

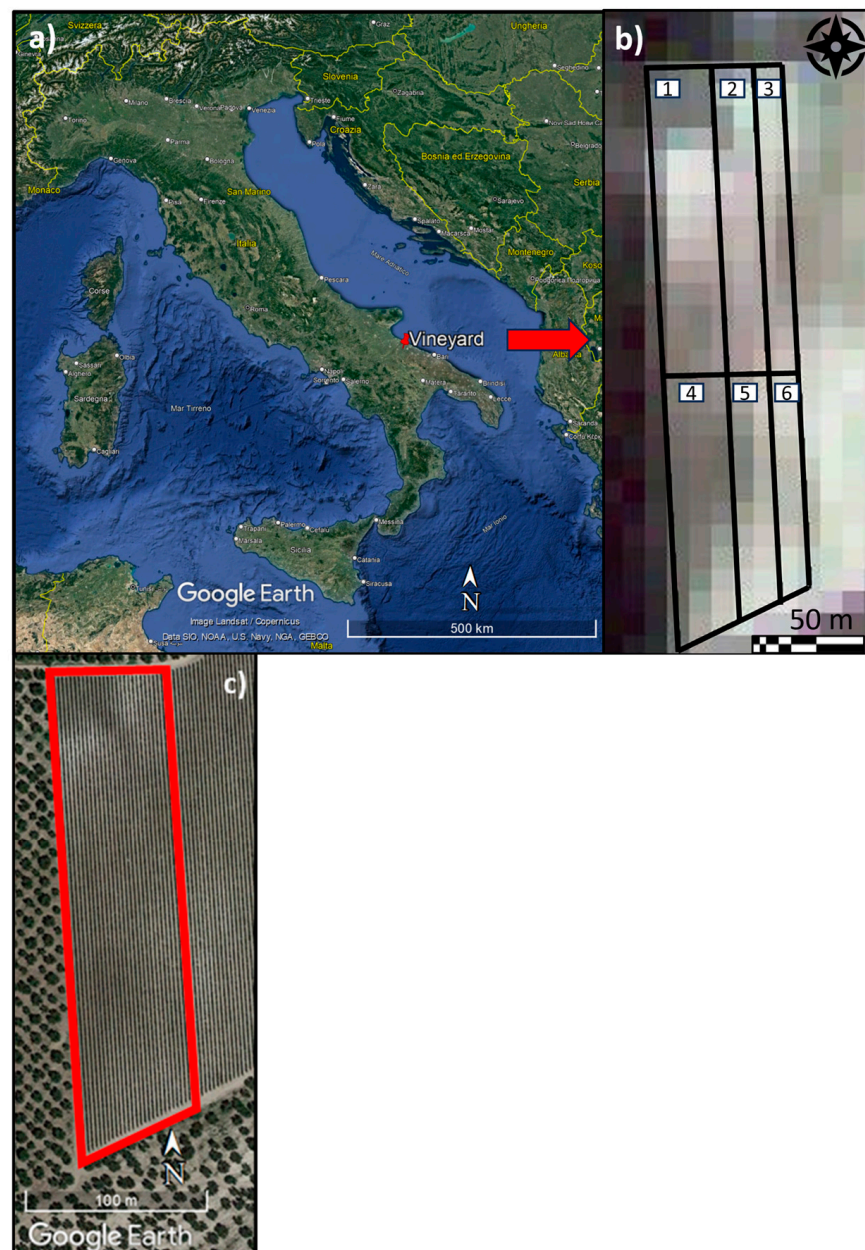


**Figure 1.** Location of the experimental vineyard in Italy (a), Sentinel-2 image of the plots where stem water potential values were acquired in 2019 and 2020 within the vineyard. Per each plot the reflectance value of the pixels was averaged (b), and Google Earth image of the vineyard (c). Google Earth Pro© and Sentinel-2 images©.

For each plot, within the same spectral band, we extracted the mean value of the reflectance of all the pixels, as well as VIs and biophysical parameters. If there was no direct temporal match between the dates of image acquisition and field data collection, we employed linear interpolation to bridge the gap, utilizing the nearest images chronologically.

**Table 1.** Vegetation indices (VIs) used in this study to predict vineyard SWP.

VIs		Equation	Reference
Leaf Area Index	LAI	SNAP—biophysical processor	[24]
Fraction Vegetation Cover	FVC	SNAP—biophysical processor	
Normalized Difference Vegetation Index	NDVI	$(B8 - B4)/(B8 + B4)$	[25]
Enhanced Vegetation Index	EVI	$2.5 * (B8 - B4)/(B8 + (6 * B4) - (7.5 * B2) + 1)$	[14]
Green Normalized Difference Vegetation Index	GNDVI	$(B8 - B3)/(B8 + B3)$	
Soil Adjusted Vegetation Index	SAVI	$(1 + 0.5) * (B8 - B4)/(B8 + B4 + 0.5)$	
Normalized Moisture Stress Index	NMSI1	$(B8 - B11)/(B8 + B11)$	
Normalized Moisture Stress Index	NMSI2	$(B8 - B12)/(B8 + B12)$	
CRI700	CRI2	$(1/B2) - (1/B5)$	[26]
Chlorophyll Green	CHLgreen	$(B7/B3)^{-1}$	[27]
Chlorophyll Red-Edge	CHLrededge	$(B7/B5)^{-1}$	
Linear Red-Edge Index	LREI	$700 + 40 * (((B4 + B7)/2) - B5)/(B6 - B5)$	
Modified Chlorophyll absorption in reflectance	MCARI	$((B5 - B4) - 0.2 * (B5 - B3)) * (B5/B4)$	
Modified Simple Ratio	MSR	$(B8/B4 - 1)/((B8/B4)^{1/2} + 1)$	
Ratio Difference Vegetation Index	RDVI	$(B8 - B4)/((B8 + B4)^{0.5})$	
Atmospherically Resistant Vegetation Index	ARVI	$(B8A - B04 - 0.106 * (B04 - B02))/(B8A + B04 - 0.106 * (B04 - B02))$	
Modified Soil Adjusted Vegetation Index	MSAVI	$MSAVI = (2 * B08 + 1 - \sqrt{(2 * B08 + 1)^2 - 8 * (B08 - B04)}) / 2$	[28]
Infrared Percentage Vegetation Index	IPVI	$B8/(B8 + B4)$	
Weighted Difference Vegetation Index	WDVI	$B8 - 0.5 * B4$	
Transformed NDVI	TNDVI	$((B8 - B4)/(B8 + B4) + 0.5)^{0.5}$	
Simple Ratio 1	SR1	$B8/B11$	[29]
Simple Ratio 2	SR2	$B8/B12$	
Normalized Difference Red-Edge	NDRE 1	$(B8 - B5)/(B8 + B5)$	
Normalized Difference Red-Edge	NDRE 2	$(B8 - B6)/(B8 + B6)$	
Inverted Red-Edge Chlorophyll Index	IRECI	$(B8 - B4)/(B5/B6)$	
Red-Edge Chlorophyll Absorption Index	RECAI	$(B8 - B6)/B3 * (B6/B3)$	
Red-Edge Position	REP	$((B4 + B8)/2) - B5)/(B6 - B5)$	

#### 2.4. Statistical and Machine Learning Analysis

To predict ΨSTEM as a function of Sentinel-2 derived variables, we tested two groups of predictors: (1) a dataset containing the median values of all Sentinel-2 bands extracted over the field plots, 10 predictors; (2) a dataset containing the median values of all Sentinel-2 VIs extracted over the field plots, 27 predictors. The two datasets were tested separately, and we did not attempt to calibrate a model using both (1) and (2) datasets together to reduce the risk of overfitting. The dataset (n = 162) was randomly divided into a training (80%) and a validation (20%) dataset [30] containing 132 and 30 observations, respectively. The training dataset was used to fit all the models developed in this study while the testing dataset was used to test the goodness of fit of each predictive model.

In this work, the compared models were lasso, ridge, elastic net, and random forest. Lasso regression is a regularization technique that improves linear regression by performing variable selection and coefficient shrinkage through the application of an L1 penalty, which

drives some coefficients exactly to zero, thus selecting a subset of relevant features [31]. Ridge regression addresses multicollinearity in linear regression models by introducing a penalty term proportional to the square of the magnitude of the coefficients (L2). This approach reduces the coefficients towards zero without exactly zeroing them, thus reducing variance and improving model stability [32]. Both lasso and ridge are widely adopted in agricultural prediction tasks [33–36]. Elastic net is a regularized regression technique that combines L1 (lasso) and L2 (ridge) penalties to improve model performance and reduce overfitting [37]. Random forest (RF) is an ensemble learning technique that improves regression trees by combining a large number of decision trees. Such technique is widely used in remote sensing and agriculture studies due to its high accuracy and ability to find non-parametric relationships [38]. In addition, unlike other machine learning techniques, RF has the advantage of relying on various methods to estimate the variable importance of each predictor variable. In our study, we used RF models implemented in the “ranger” package [39] within the R environment software (v. 4.4.2) [40]. To facilitate the fine-tuning of the models we additionally used the “caret” package [41]. In the ranger implementation of RF, we needed to fine-tune the number of trees, the number of variables to possibly split each node (“mtry”), the splitting rule, and the minimum node size. We ran our model calibration multiple times using various combinations of the above-mentioned parameters, with the exception of the number of trees, as it was not influential in the overall performance of the models; hence, we set the number of trees to 500. The variable importance was assessed through permutation [42,43]. For each run, one variable was excluded from the predictors set and the increase in model prediction error was calculated. The resulting values were then scaled from 0 to 100. Additionally, a linear model was calibrated for each one of the groups of predictors to compare the results to the lasso, ridge, elastic net, and RF models. To compare the results of the modeling procedures and their robustness, coefficient of determination ( $R^2$  (1)), root mean square error (RMSE (2)), normalized root mean square error (nRMSE (3)), and mean absolute error (MAE (4)) were calculated as follows:

$$R^2 = 1 - \frac{\sum_{i=1}^n (E_i - P_i)^2}{\sum_{i=1}^n (E_i - \bar{E}_i)^2} \quad (1)$$

$$RMSE = \sqrt{\frac{1}{n} \sum_{i=1}^n (P_i - E_i)^2} \quad (2)$$

$$nRMSE = 100 \frac{\sqrt{\frac{1}{n} \sum_{i=1}^n (P_i - E_i)^2}}{(\max(E) - \min(E))} \quad (3)$$

$$MAE = \frac{\sum_{i=1}^n |P_i - E_i|}{n} \quad (4)$$

where “P” are the predicted values, “E” the expected values and “n” the number of the observations.

Moreover, the robustness of the models has been evaluated through a 10-time repeated 5-fold cross validation.

Lastly, the RF model was applied to Sentinel-2 spectral images in order to model the temporal trend of the vineyard ΨSTEM.

RStudio software (v. 2024.12.0+467; RStudio Team, 2020, PBC, Boston, MA, USA) and SigmaPlot (SigmaPlot, Systat Software Inc., Palo Alto, CA, USA; Version 14) were used to carry out analyses, modeling, and graph plotting. Figure 2 summarizes the workflow of the study, including data collection, image processing, modelling approaches, evaluation metrics, and the generation of predictive outputs.

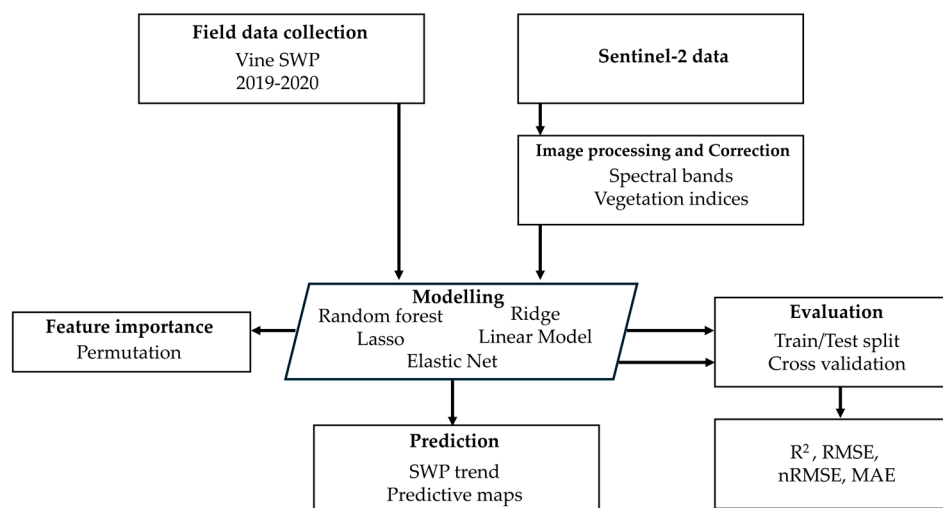


**Figure 2.** Workflow of the methodology used for predicting vine stem water potential (SWP) using Sentinel-2 data.

### 3. Results

#### 3.1. Agrometeorological Data and Vine Water Status

During the vegetative seasons of both 2019 and 2020, August was the hottest month, with an average temperature of 26.2 °C in 2019 and 26.5 °C in 2020. The total amount of rainfall in 2019 was 374.5 mm and 321.2 mm in 2020, while the rainfall amount in the irrigation seasons (from June to September) was 123 mm in 2019 and 103.2 mm in 2020. In the 2019 irrigation season, the driest month was August (0.2 mm), while, in 2020, it was June (13.6 mm); in May, July, and September of 2019, rainfall peaks occurred with 93, 57, and 56 mm, respectively (Figure 3). The highest values of ETo during 2019 were found in June and July (170 and 166 mm, respectively), whereas, during 2020, there were in July and August (191 and 170 mm, respectively) (Figure 3).

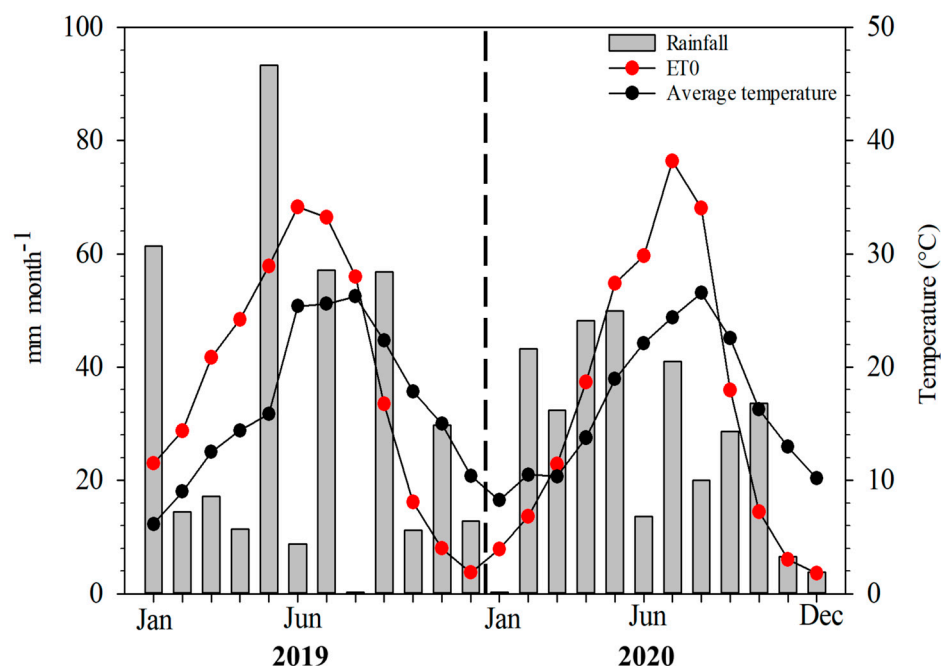


**Figure 3.** Monthly trend of average temperature, amount of rainfall, and reference evapotranspiration calculated following the equation proposed by Hargreaves–Samani [44] for the two years of the experiment around the area of the vineyard.

The average  $\Psi_{STEM}$  had a different trend in the two years of the experiment. In 2019, average  $\Psi_{STEM}$  remained stable over values of  $-1.00$  MPa until the phenological phase “berries begin to color and enlarge”, then reached average values of  $-1.41$  Mpa and  $-1.33$  Mpa during the phases of “veraison” and “ripening”, respectively; during the “pre-harvest” phase, it dropped to  $-0.99$  MPa. The highest average  $\Psi_{STEM}$  was recorded at the phenological phase “beginning of bunch closure” ( $-0.61$  MPa). In 2020, average  $\Psi_{STEM}$  ( $n = 66$ ) was over  $-1.00$  MPa only during the phenological phase “pea size”, then average  $\Psi_{STEM}$  was lower than  $-1.00$  MPa from “beginning of bunch closure” to the end of the irrigation season; the highest average  $\Psi_{STEM}$  was recorded during the phase “pea size” ( $-0.59$  MPa), the lowest average  $\Psi_{STEM}$  values occurred at the “veraison” and “ripening” phases ( $-1.23$  MPa and  $-1.27$  MPa, respectively), as in the 2019 irrigation season. Figure 4 reports the boxplot showing the distribution of the  $\Psi_{STEM}$  during the different phenological phases in the two years considered; particularly, pronounced differences in the distribution of the  $\Psi_{STEM}$  data between the two years were observed in the early phenological stages (pea size, beginning of bunch closure, and berries still hard and green).

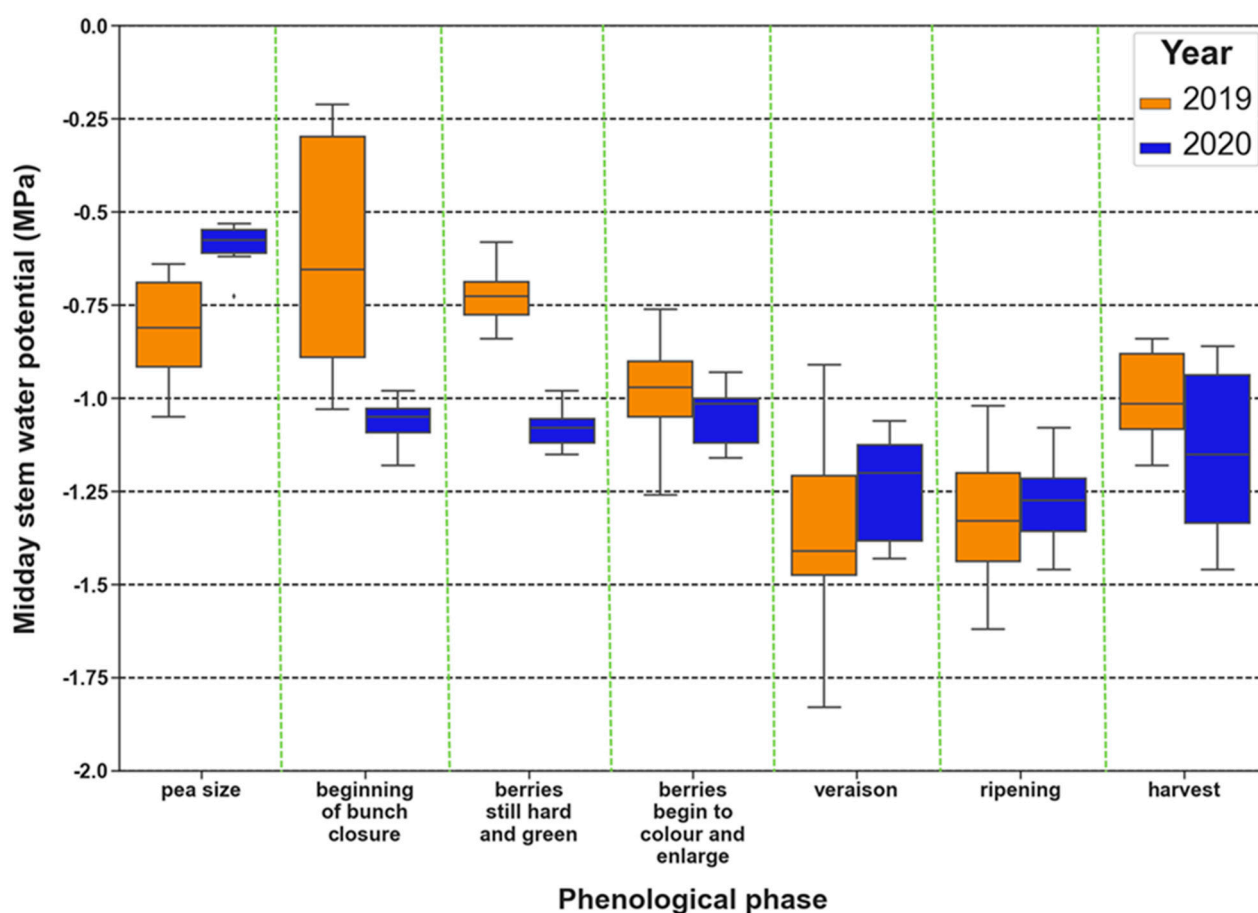


**Figure 4.** Boxplot of stem water potential during the different phenological phases in the two years of the experiment (according to Lorenz et al. [45]); whiskers indicate maximum and minimum values, and the horizontal line within the boxplot represents the median.

### 3.2. Models Evaluation

Among the compared models, RF had the higher performance in predicting  $\Psi_{STEM}$  (Table 2) and showed good fit in training when considering both VIs and spectral bands as predictors (VIs,  $R^2 = 0.95$ ; spectral bands,  $R^2 = 0.91$ ), with little errors (VIs, nRMSE = 4.3%; spectral bands, nRMSE = 5.5%). RF had better performance in testing when VIs were used as predictors, considering the  $R^2$  (VIs,  $R^2 = 0.72$ ; spectral bands  $R^2 = 0.58$ ) and the nRMSE (VIs, nRMSE = 12.4%; spectral bands, nRMSE = 15.1%) (Figure 5). These results are



further confirmed by the cross-validation (RF: VIs  $R^2 = 0.66$ ; spectral bands  $R^2 = 0.59$ ); in Supplementary Material, the complete results of the cross validation for all the evaluated models are reported (Table S1, Figure S1). Figure 6 shows the results of the optimization of the RF parameters: based on the lowest RMSE, 1 as minimum node size, extratrees as splitting rule, and four variables as mtry were used in the final modeling procedure involving spectral bands as predictors; meanwhile, 1 as minimum node size, extratrees as splitting rule, and five variables as mtry were used in the final modeling procedure involving VIs as predictors. Figure 7 shows the results of the permutation procedure to assess the importance of the variables; using the spectral bands as predictors, the most important were Vegetation Red Edge and SWIR (B7 and B12); using the VIs as predictors, the most important were IRECI and NMSI1 and NMSI2. Red band and GNDVI had no importance in modeling (0%).

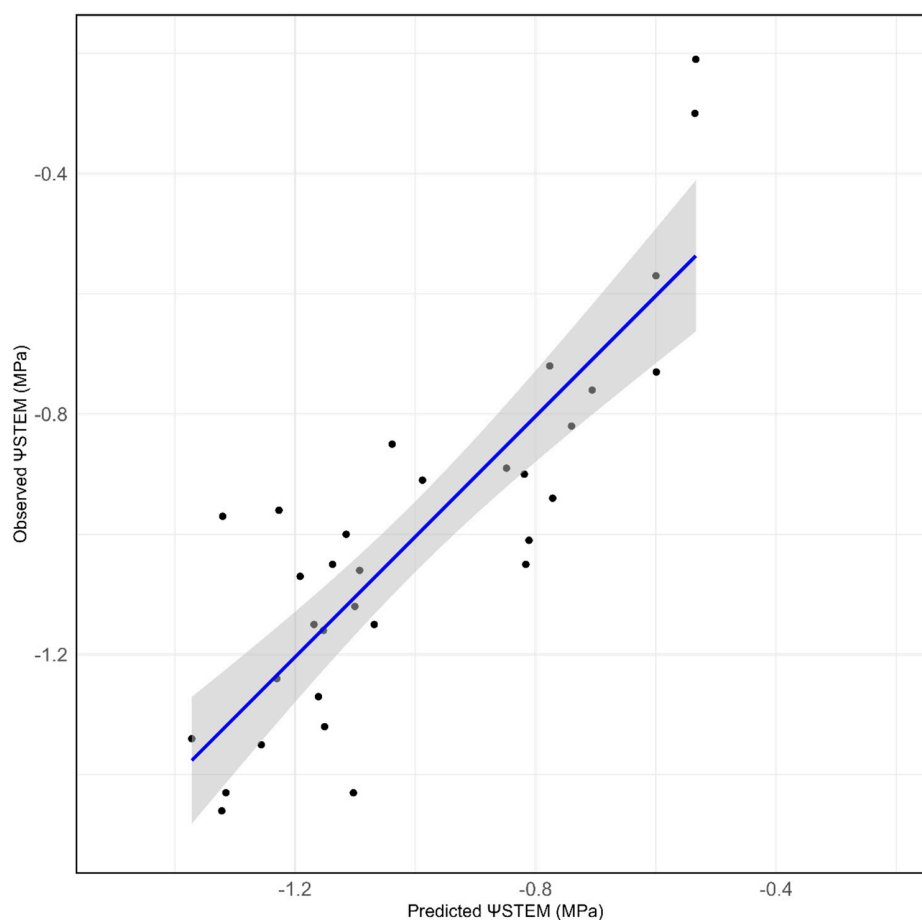


**Figure 5.** Scatterplot of the predicted and the observed values (validation dataset) of stem water potential ( $\Psi_{STEM}$ ; MPa).

**Table 2.** Performance parameters of lasso, ridge, elastic net (EN), random forest (RF), and linear model (LM) predicting vineyard stem water potential with vegetation indices (VIs) and spectral bands as predictors.

Model	Predictors	Calibration				Testing			
		$R^2$	RMSE	nRMSE	MAE	$R^2$	RMSE	nRMSE	MAE
Lasso	VIs	0.52	0.19	12.7%	0.15	0.46	0.21	17.2%	0.16
	Spectral Bands	0.45	0.21	13.7%	0.16	0.38	0.23	18.4%	0.17

Table 2. Cont.

Model	Predictors	Calibration				Testing			
		R <sup>2</sup>	RMSE	nRMSE	MAE	R <sup>2</sup>	RMSE	nRMSE	MAE
Ridge	VI <sub>s</sub>	0.50	0.20	13%	0.15	0.45	0.21	17.3%	0.16
	Spectral Bands	0.41	0.22	14.2%	0.17	0.39	0.23	18.2%	0.18
EN	VI <sub>s</sub>	0.57	0.18	12.1%	0.14	0.49	0.20	16.7%	0.16
	Spectral Bands	0.45	0.21	13.7%	0.16	0.37	0.23	18.5%	0.17
RF	VI <sub>s</sub>	0.95	0.07	4.3%	0.50	0.72	0.15	12.4%	0.12
	Spectral Bands	0.91	0.08	5.5%	0.60	0.58	0.19	15.1%	0.14
LM	VI <sub>s</sub>	0.63	0.18	11.3%	0.14	0.49	0.21	16.8%	0.16
	Spectral Bands	0.47	0.21	13.5%	0.15	0.35	0.24	18.9%	0.16

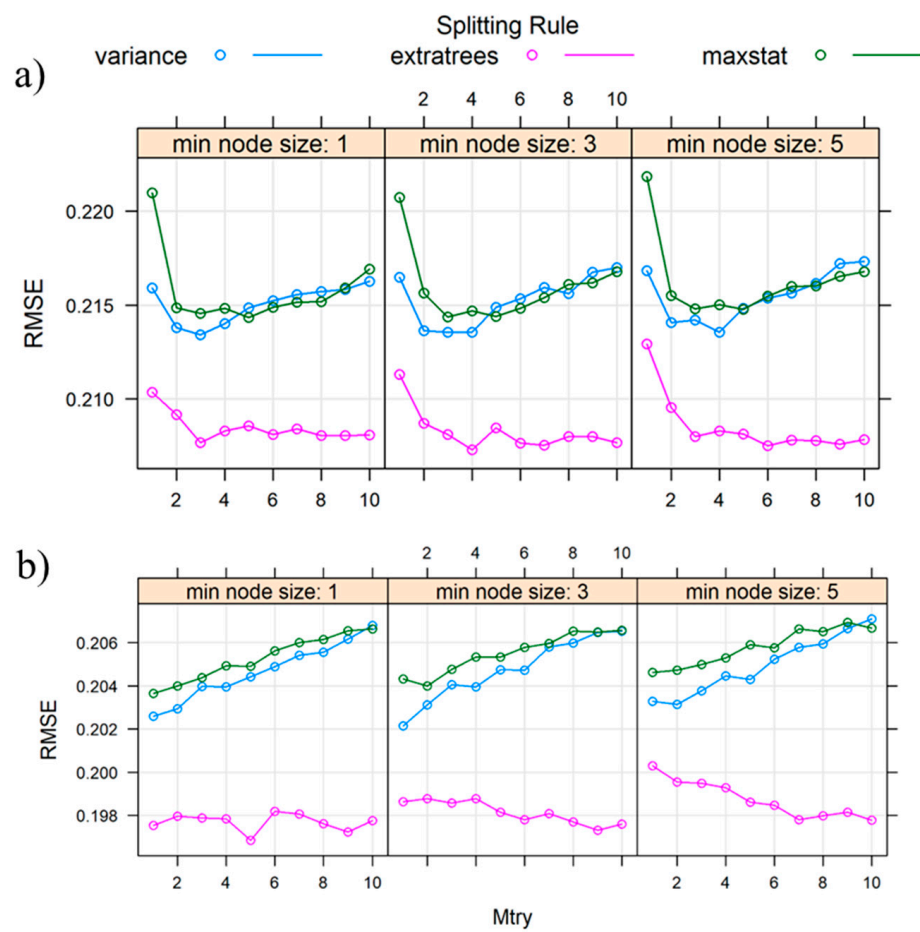
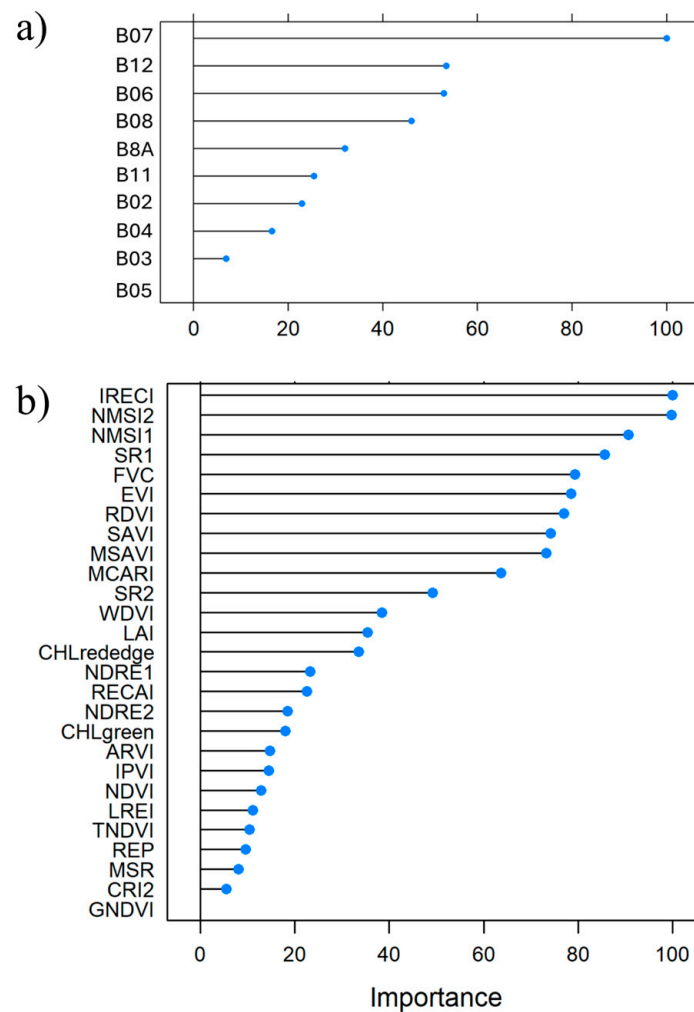


Figure 6. Optimization of random forest parameters for the models with S-2 bands (a) and the calculated VIs as predictors (b) (min node size; mtry and splitting rule).

In the prediction of  $\Psi_{STEM}$ , the other modeling approaches had lower performance compared to RF. Lasso, ridge, elastic net, and LM showed a low fit in training and testing, both considering VIs and spectral bands as predictors. The LM model trained with the spectral bands was the model that showed the lowest performance in testing (spectral bands,  $R^2 = 0.35$ ,  $nRMSE = 18.9\%$ ) (Table 2).



**Figure 7.** Results of permutation procedure to assess variable importance of the models with S-2 bands (a) and the calculated VIs (b) as predictors.

### 3.3. Remote Sensing Vine Water Status Modeling and Predictive Maps

Figure 8 contains the graphs showing the predicted  $\Psi_{STEM}$  trend in both years of the experiment, made by using the RF-based model with VIs as predictors. The predicted  $\Psi_{STEM}$  had frequent fluctuations in the first part of the 2019 irrigation season until the end of July; the lowest value reached was at the beginning of June ( $\sim -1.15$  MPa), the highest was in mid-July ( $\sim -0.65$  MPa), which was the highest of the whole season. Predicted  $\Psi_{STEM}$  sharply dropped to lower values ( $-1.25$  MPa) in the first decade of August, then fluctuated in a range between  $-1.10$  MPa and  $-1.25$  MPa. There were two abrupt increases in the first decade of September and mid-October (Figure 8a).

At the beginning of the 2020 irrigation season, the predicted  $\Psi_{STEM}$  had high values reaching values of  $\sim -0.70$  in the second half of July; the predicted  $\Psi_{STEM}$  markedly decreased in the last days of June to  $\sim -1.20$ . The lowest value of predicted  $\Psi_{STEM}$  was recorded in mid-July ( $\sim -1.27$  MPa). Until October, predicted  $\Psi_{STEM}$  values remained stable in a range between  $-1.10$  MPa and  $-1.20$  MPa; in mid-October, it sharply increased, and, thereafter, it slightly decreased to  $\sim -0.95$  (Figure 8b). Figure 9 shows the spatial variability of vineyard  $\Psi_{STEM}$ ; the predictive maps were made by applying the RF-based model to the Sentinel-2 images for two dates, 18 August 2019 and 20 August 2019.

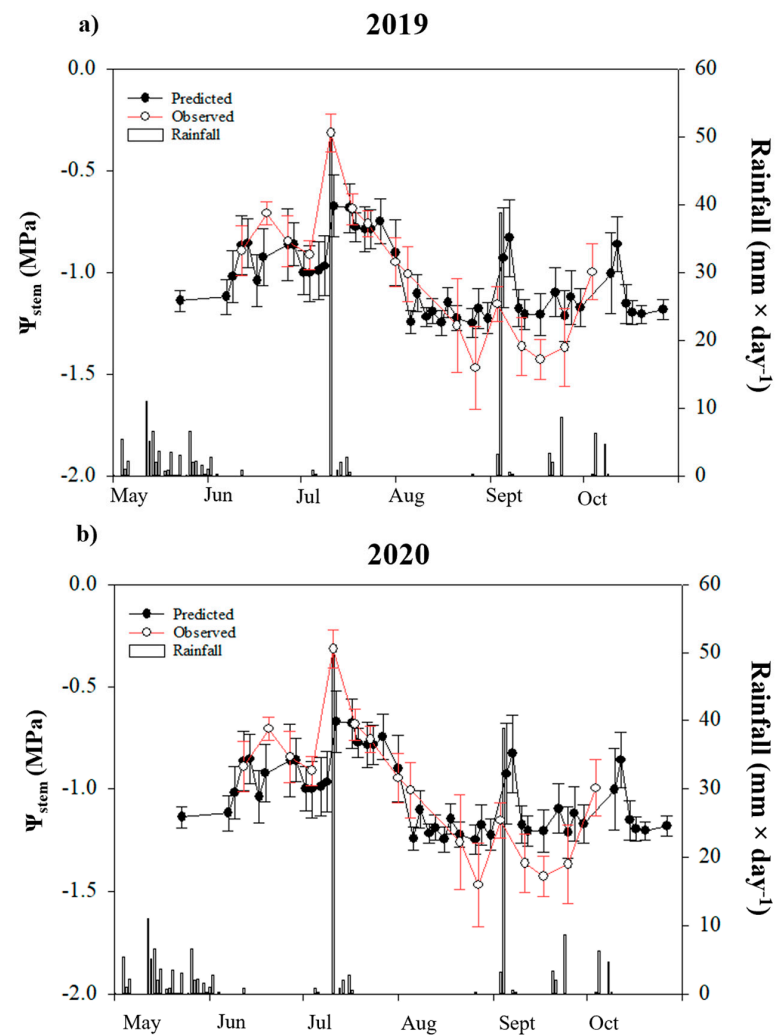


Figure 8. Daily rainfall in the area of the experiment and stem water potential in 2019 (a) and 2020 (b).

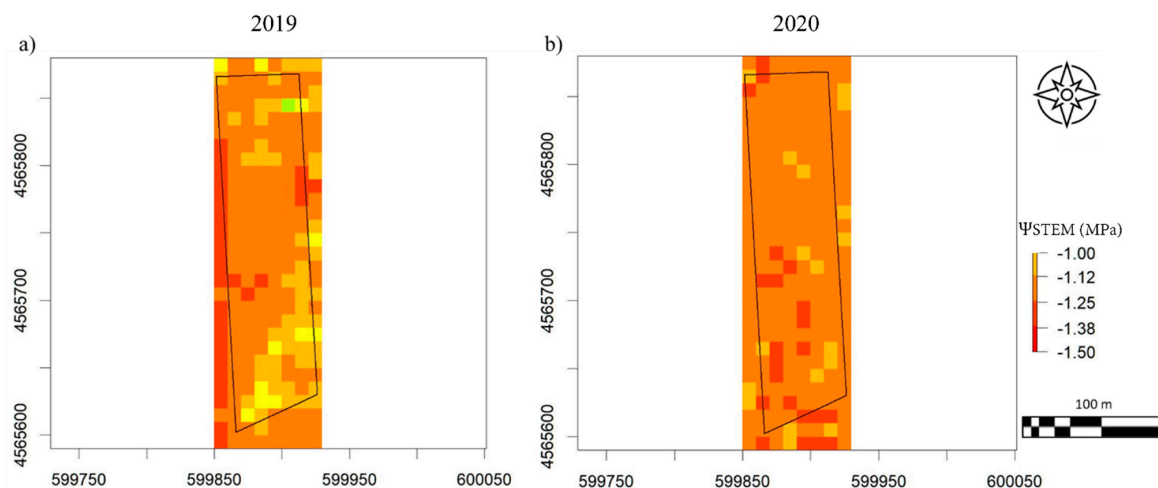


Figure 9. Predictive maps of the vineyard stem water potential ( $\Psi_{STEM}$ ) produced by applying the RF-based model trained with vegetation indices as predictors to Sentinel-2 images. Maps are referred to 18 August 2019 (a) and 20 August 2019 (b). The 95% confidence intervals for  $\Psi_{STEM}$  predictions ranged from  $-1.77$  to  $-0.19$  MPa; the plot of the 95% confidence interval for the RF model predictions (test set) is reported in Supplementary Material (Figure S2).

#### 4. Discussion

Crop monitoring is a key factor in understanding the response of plants to the environment and agronomic practices; nonetheless, it requires time-consuming fieldwork and efforts in order to obtain sufficiently representative data. Remote sensing could offer the possibility to investigate important environmental key-factors and plant response reducing fieldwork [46–49]; for instance, Bellvert et al. [19] used remote sensing to monitor crop water stress index in a Pinot-noir vineyard. In the presented study, an integration of remote sensing and machine learning was proposed to understand the temporal variability of the vineyard ΨSTEM.

The RF-based modeling approach, considering VIs as predictors, had the best results in terms of predictive performance, compared with the RF model with spectral bands as predictors and the lasso, ridge, elastic net and LM models. Machine learning approaches are widely used in agriculture for solving several problems, improving water management and water use efficiency too [50,51]. Unlike linear models, RF does not rely on strict assumptions about input–output relationships and can effectively handle the complex interplay of reflectance at different wavelengths and vegetation indices (e.g., Ceccato et al., [52]; Clevers and Kooistra, [53]). This flexibility allows RF to identify subtle spectral signatures linked to plant water stress without explicitly requiring prior knowledge of the underlying biophysical processes, a well-known advantage in machine learning applications in remote sensing [54]. As a machine learning algorithm, RF has been used to solve classification problems; however, few studies have focused on its application in regression problems [54,55]; for example, RF was used by Mpakairi et al. [56] to characterize irrigated and rainfed croplands, obtaining good results in terms of classification accuracy (0.77). For the prediction of continuous data in agricultural remote sensing applications, RF has been used by Lee et al. [57] to predict nitrogen content in corn using UAV images with notable results ( $R^2 = 0.85$ ). Moreover, in a work from Campi et al. [13], RF outperformed other machine learning algorithms in predicting peach tree ΨSTEM from satellite data ( $R^2 = 0.62$ ). In our study, the validity of RF as a predictive model was confirmed; furthermore, we compared RF with lasso, ridge, elastic net, and LM performances, and our results confirmed those found in literature, when RF was compared with linear models in remote sensing application [58,59]. The results of the permutation process suggest that, in the ΨSTEM prediction, IRECI was the most important VI, B07 (vegetation red edge band) was the most important band; IRECI is a VI, and was calculated by considering the reflectance in the red edge spectral region. Although our best model was the one that included only the indices rather than the individual bands, it remains crucial to interpret the spectral signals in terms of well-established absorption features and their underlying relationships to vegetation physiology. The red-edge spectral region, which includes Sentinel-2 bands B05, B06, and B07, is recognized for its sensitivity to changes in leaf chlorophyll, internal structure, and water content [60,61]. The vegetation indices identified as most important in our model—specifically, the Inverted Red-Edge Chlorophyll Index (IRECI), and the Normalized Moisture Stress Indices (NMSI1 and NMSI2)—draw heavily on the same spectral regions (red-edge and SWIR) that showed strong importance at the band level. IRECI exploits the red-edge region to capture chlorophyll and structural variations sensitive to drought stress, while NMSI1 and NMSI2 incorporate NIR and SWIR bands, providing direct sensitivity to leaf moisture conditions. The SWIR region is known to be sensitive to leaf water absorption features, providing an integrated response to changes in plant moisture status [52]. By combining red-edge and SWIR reflectance properties, both at the band level and within the most predictive indices (IRECI, NMSI1, NMSI2), we capture a comprehensive spectral signature of vine water status. The synergy between these spectral domains and the derived indices underlines how the spectral sensitivities to water content and structural changes are integrally reflected within the key VIs identified using the RF model. Satellite data have been used to assess water productivity in agriculture, e.g., Teixeira et al. [62] used Landsat 8 images to quantify water productivity in coconut; however, the advantage of using Sentinel-2 images rather than Landsat 8 is

undoubtedly the spatial resolution of the images, which is higher for Sentinel-2 images than Landsat 8. Van Beek et al. [63] used WorldView 2 satellite data to predict  $\Psi$ STEM in pear orchards with promising results; Helman et al. [14] used Planet satellite imagery and linear model to predict vineyard  $\Psi$ STEM with one-year data from 82 vineyard and Vis time series, obtaining interesting results ( $R^2 = 0.60$ ). WorldView 2 and Planet images certainly offer a considerable advantage in terms of spatial resolution; however, it should be taken into consideration that spectral images from these satellite platforms are not available for free, as, for Sentinel-2 and Landsat 8, this could greatly reduce the applicability of these technologies at a farm level [64]. Sentinel-2 images have already been used to predict vineyard  $\Psi$ STEM by Laroche-Pinel et al. [16]. In their research, they obtained good results with a Bayesian model ( $R^2 = 0.40$  and RMSE = 0.26 MPa) but lower than those obtained in our study.

Considering the satisfying results in the prediction of  $\Psi$ STEM, we applied the RF-based model to predict the trend of  $\Psi$ STEM during the two irrigation seasons. In the 2019 irrigation season, predicted  $\Psi$ STEM sharply dropped in mid-June, and this could be linked to high ETo and low amount of rainfall in June [65,66]; therefore, in July, there was a considerable increase in the predicted  $\Psi$ STEM. In fact, in July, there was a significant amount of rainfall. In August, with almost no precipitation, predicted  $\Psi$ STEM sharply decreased. In the 2020 irrigation season, the predicted  $\Psi$ STEM showed a sudden lowering at the end of June, then remained around  $-1.2$  MPa almost until the end of the irrigation season, even if the amount of rainfall was better distributed during the irrigation season in 2020 than 2019, with precipitation in August too. This could be explained by higher ETo, especially in July.  $\Psi$ STEM of  $-1.2$  MPa is generally considered a threshold between moderate to severe water stress in viticulture [67]; therefore, by considering the built predictive model, it could be stated that the vineyard under study has experienced more pronounced drought stress in 2020 than 2019, as well as for a longer period during the irrigation season. Doubtlessly, to discuss  $\Psi$ STEM trends in more detail, it is necessary to know all the field conditions, particularly the amount of water in the rhizosphere and the dynamics of water movement in the soil, as well as solar radiation in that area [68–70]; however, such arguments are outside the scope of this study.

This work demonstrated that, in combination with machine learning, it is possible to use Sentinel-2 imagery to extend the information of  $\Psi$ STEM data measured in random locations within the vineyard to unseen locations. In other words, it uses contemporary satellite spectral data as ancillary variables to produce maps from a finite number of measurements. The developed model could be used to assist farmers in monitoring the water status variability within the field and then check whether the irrigation practice may need adjustment; nonetheless, some limitations, must be taken into account, such as the spatial resolution of the Sentinel-2 images and frequency of image acquisition. While our model demonstrated robust performance in predicting vine water status, it is important to recognize the limitations posed by the relatively small dataset (162 data points) collected from a single vineyard. This limitation restricts the diversity of environmental conditions and vineyard management practices represented in the model, which could impact its generalizability. Additional work could confirm these results, for example, by considering other vine cultivars and growing systems, increasing the sample size, using data from vineyards with different locations to enhance the variability in the dataset for the modeling process, and exploring the integration of higher spatial resolution remote sensing platforms (e.g., WorldView or PlanetScope) alongside Sentinel-2 imagery to evaluate their potential advantages and complementarity. Furthermore, although random forest demonstrated good performance, its nonlinear nature introduces a potential risk of overfitting, particularly with small datasets. To address this, we implemented extensive cross-validation and hyperparameter tuning.

## 5. Conclusions

In this study, an innovative approach based on the combination of satellite remote sensing and machine learning has been proposed for the estimation of vine water status. It has been shown that the accuracy of the random forest algorithm increases when vegetation indices are used as predictors of the stem water potential instead of the reflectance of the spectral bands. Furthermore, both random forest-based modeling approaches had better performance than the lasso, ridge, elastic net, and LM models. The permutation process confirmed the importance of the reflectance in the red edge spectral region in plant water status monitoring and drought stress response. The results show that the integration of remote sensing and machine learning could provide a useful tool for vine water status management, especially as an alternative or addition to typical proximal field measurements.

**Supplementary Materials:** The following supporting information can be downloaded at: <https://www.mdpi.com/article/10.3390/rs16244784/s1>, Figure S1: Boxplots showing the distribution of the performance parameters of random forest in predicting vine stem water potential across 10 repetitions of the 5-fold cross validation, using the vegetation indices (a) and Sentinel-2 spectral bands (b) as predictors; Figure S2: Prediction intervals for soil water potential (SWP, MPa) using the random forest (RF) model trained with the vegetation indices, with 95% confidence intervals (CIs). The blue points represent the predicted values, while the red error bars denote the upper and lower bounds of the out of bag-derived 95% CIs; Table S1: Results of the 10-times repeated 5-fold cross-validation used to assess the robustness of Lasso, Ridge, elastic net (EN), random forest (RF), and linear model (LM) in vine stem water potential prediction. VIs = vegetation indices; S2Bs = Sentinel-2 spectral bands.

**Author Contributions:** V.G.: Writing—original draft, Conceptualization, Methodology, Investigation, Data curation, Formal analysis, Software, Visualization. S.P.G.: Writing—original draft, Data curation, Software, Visualization. L.B.: Writing—review and editing. P.S.: Writing—review and editing. M.E.: Writing—review and editing. G.L.: Writing—review and editing. S.C.: Writing—review and editing. R.L.: Writing—review and editing. G.S.: Writing—review and editing. G.A.V.: Conceptualization, Funding acquisition, Project administration, Supervision, Methodology, Investigation, Writing—review and editing. All authors have read and agreed to the published version of the manuscript.

**Funding:** This paper was supported by the TEBAKA project (TERRitorial BASic Knowledge Acquisition project) “Avviso MIUR n. 1735 del 13/07/2017”, Programma di finanziamento: Programma Operativo Nazionale “Ricerca e Innovazione” 2014–2020 (PON “R&I” 2014–2020). ARS01\_00815 (CUP B82C20000160005).

**Data Availability Statement:** The original contributions presented in this study are included in the article/Supplementary Material. Further inquiries can be directed to the corresponding author.

**Conflicts of Interest:** Author Pietro Sciusco was employed by the company Planetek Italia. The remaining authors declare that the research was conducted in the absence of any commercial or financial relationships that could be construed as a potential conflict of interest.

## References

1. Calvin, K.; Dasgupta, D.; Krinner, G.; Mukherji, A.; Thorne, P.; Trisos, C.; Romero, J.; Aldunce, P.; Barrett, K.; Blanco, G.; et al. *Climate Change 2023: Synthesis Report*; Lee, H., Romero, J., Eds.; Contribution of Working Groups I, II and III to the Sixth Assessment Report of the Intergovernmental Panel on Climate; IPCC: Geneva, Switzerland, 2023. [\[CrossRef\]](#)
2. Gomez-Zavaglia, A.; Mejuto, J.C.; Simal-Gandara, J. Mitigation of emerging implications of climate change on food production systems. *Food Res. Int.* **2020**, *134*, 109256. [\[CrossRef\]](#) [\[PubMed\]](#)
3. Van Leeuwen, C.; Destrac-Irvine, A. Modified grape composition under climate change conditions requires adaptations in the vineyard. *Oeno One* **2017**, *51*, 147–154. [\[CrossRef\]](#)
4. Van Leeuwen, C.; Destrac-Irvine, A.; Dubernet, M.; Duchêne, E.; Gowdy, M.; Marguerit, E.; Pieri, P.; Parker, A.; De Rességuier, L.; Ollat, N. An update on the impact of climate change in viticulture and potential adaptations. *Agronomy* **2019**, *9*, 514. [\[CrossRef\]](#)
5. Costa, J.M.; Vaz, M.; Escalona, J.; Egipto, R.; Lopes, C.; Medrano, H.; Chaves, M.M. Modern viticulture in southern Europe: Vulnerabilities and strategies for adaptation to water scarcity. *Agric. Water Manag.* **2016**, *164*, 5–18. [\[CrossRef\]](#)

6. Guilpart, N.; Metay, A.; Gary, C. Grapevine bud fertility and number of berries per bunch are determined by water and nitrogen stress around flowering in the previous year. *Eur. J. Agron.* **2014**, *54*, 9–20. [[CrossRef](#)]
7. Irvin Ojeda, H. Influence of pre-and post-veraison water deficit on synthesis and concentration of skin phenolic compounds during berry growth of *Vitis vinifera* cv. Shiraz. *Am. J. Enol. Vitic.* **2014**, *53*, 261–267.
8. Virnodkar, S.S.; Pachghare, V.K.; Patil, V.C.; Jha, S.K. Remote sensing and machine learning for crop water stress determination in various crops: A critical review. *Precis. Agric.* **2020**, *21*, 1121–1155. [[CrossRef](#)]
9. Garofalo, S.P.; Intrigliolo, D.S.; Camposeo, S.; Alhaji Ali, S.; Tedone, L.; Lopriore, G.; De Mastro, G.; Vivaldi, G.A. Agronomic Responses of Grapevines to an Irrigation Scheduling Approach Based on Continuous Monitoring of Soil Water Content. *Agronomy* **2023**, *13*, 2821. [[CrossRef](#)]
10. Vuolo, F.; Essl, L.; Atzberger, C. Costs and benefits of satellite-based tools for irrigation management. *Front. Environ. Sci.* **2015**, *3*, 52. [[CrossRef](#)]
11. Alhaji Ali, S.; Vivaldi, G.A.; Garofalo, S.P.; Costanza, L.; Camposeo, S. Land Suitability Analysis of Six Fruit Tree Species Immune/Resistant to *Xylella fastidiosa* as Alternative Crops in Infected Olive-Growing Areas. *Agronomy* **2023**, *13*, 547. [[CrossRef](#)]
12. Costanza, L.; Maldera, F.; Garofalo, S.P.; Vivaldi, G.A.; Camposeo, S. Ecological optima show the potential diffusion of minor tree crops in *Xylella fastidiosa* subsp. *pauca*-infected areas through a GIS-based approach. *Front. Agron.* **2024**, *6*, 1421627. [[CrossRef](#)]
13. Campi, P.; Modugno, A.F.; De Carolis, G.; Pedrero Salcedo, F.; Lorente, B.; Garofalo, S.P. A Machine Learning Approach to Monitor the Physiological and Water Status of an Irrigated Peach Orchard under Semi-Arid Conditions by Using Multispectral Satellite Data. *Water* **2024**, *16*, 2224. [[CrossRef](#)]
14. Helman, D.; Bahat, I.; Netzer, Y.; Ben-Gal, A.; Alchanatis, V.; Peeters, A.; Cohen, Y. Using time series of high-resolution planet satellite images to monitor grapevine stem water potential in commercial vineyards. *Remote Sens.* **2018**, *10*, 1615. [[CrossRef](#)]
15. Tang, Z.; Jin, Y.; Alsina, M.M.; McElrone, A.J.; Kustas, W.P. Vine water status mapping with multispectral UAV imagery and machine learning. *Irrig. Sci.* **2022**, *40*, 715–730. [[CrossRef](#)]
16. Laroche-Pinel, E.; Duthoit, S.; Albughdadi, M.; Costard, A.D.; Rousseau, J.; Chéret, V.; Clenet, H. Towards vine water status monitoring on a large scale using sentinel-2 images. *Remote Sens.* **2021**, *13*, 1837. [[CrossRef](#)]
17. López-Pérez, E.; Sanchis-Ibor, C.; Jiménez-Bello M, Á.; Pulido-Velazquez, M. Mapping of irrigated vineyard areas through the use of machine learning techniques and remote sensing. *Agric. Water Manag.* **2024**, *302*, 108988. [[CrossRef](#)]
18. Sozzi, M.; Kayad, A.; Marinello, F.; Taylor, J.; Tisseyre, B. Comparing vineyard imagery acquired from Sentinel-2 and Unmanned Aerial Vehicle (UAV) platform. *OENO One* **2020**, *54*, 273–281. [[CrossRef](#)]
19. Bellvert, J.; Zarco-Tejada, P.J.; Girona, J.; Fereres, E. Mapping crop water stress index in a ‘Pinot-noir’ vineyard: Comparing ground measurements with thermal remote sensing imagery from an unmanned aerial vehicle. *Precis. Agric.* **2014**, *15*, 361–376. [[CrossRef](#)]
20. Cilli, R.; Elia, M.; D’Este, M.; Giannico, V.; Amoroso, N.; Lombardi, A.; Pantaleo, E.; Monaco, A.; Sanesi, G.; Tangaro, S.; et al. Explainable artificial intelligence (XAI) detects wildfire occurrence in the Mediterranean countries of Southern Europe. *Sci. Rep.* **2022**, *12*, 16349. [[CrossRef](#)]
21. Climate-Data.Org. 2024. Available online: <https://en.climate-data.org/> (accessed on 15 September 2024).
22. Protezione Civile. Sezione Protezione Civile Regione Puglia. 2024. Available online: <https://pr2127.regione.puglia.it/it/web/protezionecivile/bollettini-meteorologici-regionali-mensili> (accessed on 15 September 2024).
23. Copernicus.Eu. 2023. Available online: [https://www.esa.int/Applications/Observing\\_the\\_Earth/Copernicus](https://www.esa.int/Applications/Observing_the_Earth/Copernicus) (accessed on 11 June 2024).
24. Available online: <https://step.esa.int/main/download/snap-download/> (accessed on 11 June 2024).
25. Rouse, W.; Haas, R.H.; Deering, D.W. *Monitoring Vegetation Systems in the Great Plains with ERTS*; Third ERTS Symposium (NASA SP-351); NASA: Washington, DC, USA, 1974; Volume 1.
26. Alexandridis, T.K.; Moshou, D.; Pantazi, X.E.; Tamouridou, A.A.; Kozhukh, D.; Castef, F.; Lagopodi, A.; Zartaloudis, Z.; Mourelatos, S.; de Santos, F.J.N. Olive Trees Stress Detection Using Sentinel-2 Images. In Proceedings of the IEEE International Geoscience and Remote Sensing Symposium, Yokohama, Japan, 28 July–2 August 2019.
27. Cogato, A.; Pagay, V.; Marinello, F.; Meggio, F.; Grace, P.; Migliorati, M.D.A. Assessing the feasibility of using sentinel-2 imagery to quantify the impact of heatwaves on irrigated vineyards. *Remote Sens.* **2019**, *11*, 2869. [[CrossRef](#)]
28. Lin, Y.; Zhu, Z.; Guo, W.; Sun, Y.; Yang, X.; Kovalsky, V. Continuous monitoring of cotton stem water potential using Sentinel-2 imagery. *Remote Sens.* **2020**, *12*, 1176. [[CrossRef](#)]
29. Laroche-Pinel, E.; Albughdadi, M.; Duthoit, S.; Chéret, V.; Rousseau, J.; Clenet, H. Understanding vine hyperspectral signature through different irrigation plans: A first step to monitor vineyard water status. *Remote Sens.* **2021**, *13*, 536. [[CrossRef](#)]
30. Wang, X.; Liu, C.; van der Fels-Klerx, H.J. Regional prediction of multi-mycotoxin contamination of wheat in Europe using machine learning. *Food Res. Int.* **2022**, *159*, 111588. [[CrossRef](#)] [[PubMed](#)]
31. Tibshirani, R. Regression Shrinkage and Selection via The Lasso: A Retrospective. *J. R. Stat. Soc. Ser. B Stat. Methodol.* **2011**, *73*, 273–282. [[CrossRef](#)]
32. Venkatesh, K.A.; Mishra, D.; Manimozhi, T. Model selection and regularization. In *Statistical Modeling in Machine Learning*; Academic Press: Cambridge, MA, USA, 2023; pp. 159–178.
33. Didari, S.; Talebnejad, R.; Bahrami, M.; Mahmoudi, M.R. Dryland farming wheat yield prediction using the Lasso regression model and meteorological variables in dry and semi-dry region. *Stoch. Environ. Res. Risk Assess.* **2023**, *37*, 3967–3985. [[CrossRef](#)]



34. Guo, Y.; He, J.; Zhang, H.; Zeng, K.; Wang, L.; Chen, Z.; Zhang, Y. Predictive modeling of nitrogen content in winter wheat plants based on LASSO feature screening and UAV imagery. In Proceedings of the Fourth International Conference on Sensors and Information Technology (ICSI 2024), Xiamen, China, 5–7 January 2024; SPIE: St Bellingham, WA, USA, 2024; Volume 13107, pp. 345–354.
35. Marcillo, G.S.; Mirsky, S.; Poncet, A.; Reberg-Horton, C.; Timlin, D.; Schomberg, H.; Ramos, P. Using statistical learning algorithms to predict cover crop biomass and cover crop nitrogen content. *Agron. J.* **2020**, *112*, 4898–4913. [[CrossRef](#)]
36. Devi, M.; Malik, D.P.; Mehala, V.; Mishra, P. Measuring Variability and Factors Affecting the Agricultural Production: A Ridge Regression Approach. *Ann. Data Sci.* **2023**, *10*, 513–526. [[CrossRef](#)]
37. Lei, L.; Zheng, Q.; Dong, L.; Mo, Y.; Wang, C.; Zhang, J.; Liang, B. Improving the frequency resolution of distribution of relaxation times by integrating elastic net regularization and quantum particle swarm optimization. *Int. J. Hydrogen Energy* **2024**, *84*, 457–467. [[CrossRef](#)]
38. Garofalo, S.P.; Giannico, V.; Lorente, B.; Vivaldi, G.A.; Jose, A. Predicting Carob Tree Physiological Parameters under Different Irrigation Systems Using Random Forest and Planet Satellite Images. *Front. Plant Sci.* **2024**, *15*, 1302435. [[CrossRef](#)]
39. Wright, M.N.; Ziegler, A. Ranger: A fast implementation of random forests for high dimensional data in C++ and R. *J. Stat. Softw.* **2017**, *77*, 1–17. [[CrossRef](#)]
40. Racine, J.S. RStudio: A platform-independent IDE for R and Sweave. *J. Appl. Econom.* **2012**, *27*, 167–172. [[CrossRef](#)]
41. Kuhn, M. Building Predictive Models in R Using the caret Package. *J. Stat. Softw.* **2008**, *28*, 1–26. [[CrossRef](#)]
42. Janitzka, S.; Strobl, C.; Boulesteix, A.L. An AUC-based permutation variable importance measure for random forests. *BMC Bioinform.* **2013**, *14*, 119. [[CrossRef](#)]
43. Acharjee, A.; Larkman, J.; Xu, Y.; Cardoso, V.R.; Gkoutos, G.V. A random forest based biomarker discovery and power analysis framework for diagnostics research. *BMC Med. Genom.* **2020**, *13*, 178. [[CrossRef](#)]
44. Hargreaves, G.H.; Samani, Z.A. Reference crop evapotranspiration from temperature. *Appl. Eng. Agric.* **1985**, *1*, 96–99. [[CrossRef](#)]
45. Lorenz, D.H.; Eichhorn, K.W.; Bleiholder, H.; Klose, R.; Meier, U.; Weber, E. Growth Stages of the Grapevine: Phenological growth stages of the grapevine (*Vitis vinifera* L. ssp. *vinifera*)—Codes and descriptions according to the extended BBCH scale. *Aust. J. Grape Wine Res.* **1995**, *1*, 100–103. [[CrossRef](#)]
46. Khanal, S.; Kc, K.; Fulton, J.P.; Shearer, S.; Ozkan, E. Remote sensing in agriculture—Accomplishments, limitations, and opportunities. *Remote Sens.* **2020**, *12*, 3783. [[CrossRef](#)]
47. Mzid, N.; Boussadia, O.; Albrizio, R.; Stellacci, A.M.; Braham, M.; Todorovic, M. Salinity Properties Retrieval from Sentinel-2 Satellite Data and Machine Learning Algorithms. *Agronomy* **2023**, *13*, 716. [[CrossRef](#)]
48. Sellami, M.H.; Albrizio, R.; Čolović, M.; Hamze, M.; Cantore, V.; Todorovic, M.; Piscitelli, L.; Stellacci, A.M. Selection of Hyperspectral Vegetation Indices for Monitoring Yield and Physiological Response in Sweet Maize under Different Water and Nitrogen Availability. *Agronomy* **2022**, *12*, 489. [[CrossRef](#)]
49. Bégué, A.; Arvor, D.; Bellon, B.; Betbeder, J.; De Abelleyra, D.; Ferraz, R.P.D.; Verón, S.R. Remote sensing and cropping practices: A review. *Remote Sens.* **2018**, *10*, 99. [[CrossRef](#)]
50. Liakos, K.G.; Busato, P.; Moshou, D.; Pearson, S.; Bochtis, D. Machine learning in agriculture: A review. *Sensors* **2018**, *18*, 2674. [[CrossRef](#)]
51. Dehghanisanij, H.; Emami, H.; Emami, S.; Rezaverdinejad, V. A hybrid machine learning approach for estimating the water-use efficiency and yield in agriculture. *Sci. Rep.* **2022**, *12*, 6728. [[CrossRef](#)]
52. Ceccato, P.; Flasse, S.; Tarantola, S.; Jacquemoud, S.; Grégoire, J.-M. Detecting vegetation leaf water content using reflectance in the optical domain. *Remote Sens. Environ.* **2001**, *77*, 22–33. [[CrossRef](#)]
53. Clevers, J.G.P.W.; Kooistra, L. Using hyperspectral remote sensing data for retrieving canopy chlorophyll and nitrogen content. *IEEE J. Sel. Top. Appl. Earth Obs. Remote Sens.* **2012**, *5*, 574–583. [[CrossRef](#)]
54. Belgiu, M.; Drăgu, L. Random forest in remote sensing: A review of applications and future directions. *ISPRS J. Photogramm. Remote Sens.* **2016**, *114*, 24–31. [[CrossRef](#)]
55. Elavarasan, D.; Vincent, P.D.R. A reinforced random forest model for enhanced crop yield prediction by integrating agrarian parameters. *J. Ambient. Intell. Humaniz. Comput.* **2021**, *12*, 10009–10022. [[CrossRef](#)]
56. Mpakairi, K.S.; Dube, T.; Sibanda, M.; Mutanga, O. Fine-scale characterization of irrigated and rainfed croplands at national scale using multi-source data, random forest, and deep learning algorithms. *ISPRS J. Photogramm. Remote Sens.* **2023**, *204*, 117–130. [[CrossRef](#)]
57. Lee, H.; Wang, J.; Leblon, B. Using linear regression, random forests, and support vector machine with unmanned aerial vehicle multispectral images to predict canopy nitrogen weight in corn. *Remote Sens.* **2020**, *12*, 2071. [[CrossRef](#)]
58. López-Serrano, P.M.; López-Sánchez, C.A.; Álvarez-González, J.G.; García-Gutiérrez, J. A Comparison of Machine Learning Techniques Applied to Landsat-5 TM Spectral Data for Biomass Estimation. *Can. J. Remote Sens.* **2016**, *42*, 690–705. [[CrossRef](#)]
59. Ahmed, O.S.; Franklin, S.E.; Wulder, M.A.; White, J.C. Characterizing stand-level forest canopy cover and height using Landsat time series, samples of airborne LiDAR, and the Random Forest algorithm. *ISPRS J. Photogramm. Remote Sens.* **2015**, *101*, 89–101. [[CrossRef](#)]
60. Curran, P.J. Remote sensing of foliar chemistry. *Remote Sens. Environ.* **1989**, *30*, 271–278. [[CrossRef](#)]
61. Zarco-Tejada, P.J.; Miller, J.R.; Mohammed, G.H.; Noland, T.L. Chlorophyll Fluorescence Effects on Vegetation Apparent Reflectance. I. Leaf-Level Measurements and Model Simulation. *Remote Sens. Environ.* **2000**, *74*, 582–595. [[CrossRef](#)]

62. Teixeira, A.H.d.C.; de Miranda, F.R.; Leivas, J.F.; Pacheco, E.P.; Garçon, E.A.M. Water productivity assessments for dwarf coconut by using Landsat 8 images and agrometeorological data. *ISPRS J. Photogramm. Remote Sens.* **2019**, *155*, 150–158. [[CrossRef](#)]
63. Van Beek, J.; Tits, L.; Somers, B.; Coppin, P. Stem Water Potential Monitoring in Pear Orchards through worldview-2 Multispectral Imagery. *Remote Sens.* **2013**, *5*, 6647–6666. [[CrossRef](#)]
64. Segarra, J.; Buchailot, M.L.; Araus, J.L.; Kefauver, S.C. Remote Sensing for Precision Agriculture: Sentinel-2 Improved Features and Applications. *Agronomy* **2020**, *10*, 641. [[CrossRef](#)]
65. Patakas, A.; Noitsakis, B.; Chouzouri, A. Optimization of irrigation water use in grapevines using the relationship between transpiration and plant water status. *Agric. Ecosyst. Environ.* **2005**, *106*, 253–259. [[CrossRef](#)]
66. Jahangir, M.H.; Arast, M. Remote sensing products for predicting actual evapotranspiration and water stress footprints under different land cover. *J. Clean. Prod.* **2020**, *266*, 121818. [[CrossRef](#)]
67. Girona, J.; Mata, M.; Del Campo, J.; Arbonés, A.; Bartra, E.; Marsal, J. The use of midday leaf water potential for scheduling deficit irrigation in vineyards. *Irrig. Sci.* **2006**, *24*, 115–127. [[CrossRef](#)]
68. Nadler, A.; Raveh, E.; Yermiyahu, U.; Green, S.R. Evaluation of TDR Use to Monitor Water Content in Stem of Lemon Trees and Soil and Their Response to Water Stress. *Soil Sci. Soc. Am. J.* **2003**, *67*, 437–448. [[CrossRef](#)]
69. Oogathoo, S.; Houle, D.; Duchesne, L.; Kneeshaw, D. Vapour pressure deficit and solar radiation are the major drivers of transpiration of balsam fir and black spruce tree species in humid boreal regions, even during a short-term drought. *Agric. For. Meteorol.* **2020**, *291*, 108063. [[CrossRef](#)]
70. Suter, B.; Triolo, R.; Pernet, D.; Dai, Z.; Van Leeuwen, C. Modeling Stem Water Potential by Separating the Effects of Soil Water Availability and Climatic Conditions on Water Status in Grapevine (*Vitis vinifera* L.). *Front. Plant Sci.* **2019**, *10*, 1485. [[CrossRef](#)]

**Disclaimer/Publisher’s Note:** The statements, opinions and data contained in all publications are solely those of the individual author(s) and contributor(s) and not of MDPI and/or the editor(s). MDPI and/or the editor(s) disclaim responsibility for any injury to people or property resulting from any ideas, methods, instructions or products referred to in the content.